LA-UR--88-1671

CONF-880372--4

Los Alamos National Laboratory is operated by the University of California for the United States Department of Energy under contract W-7405-ENG-36

LA-UR--88-1671

DE88 010947

TITLE: RAMAN SPECTROSCOPY ON SIMPLE MOLECULAR SYSTEMS AT VERY HIGH DENSITY

AUTHOR(S): David Schiferl
Richard S. LeSar
David S. Moore

SUBMITTED TO: NATO Advance Research Workshop on "Simple Molecular Systems at Very High Density," Les Rouches, France, March 29, 1988 to April 6, 1988

DISCLAIMER

Los Alamos National Laboratory
Los Alamos, New Mexico 87545

RAMAN SPECTROSCOPY ON SIMPLE MOLECULAR SYSTEMS AT VERY HIGH DENSITY*

D. Schiferl, R. LeSar, and D. S. Moore

Los Alamos National Laboratory
Los Alamos, New Mexico, USA 87545

INTRODUCTION

We present an overview of how Raman spectroscopy is done on simple molecular substances at high pressures. Raman spectroscopy is one of the most powerful tools for studying these substances. It is often the quickest means to explore changes in crystal and molecular structures, changes in bond strength, and the formation of new chemical species. Raman measurements have been made at pressures up to 200 GPa (2 Mbar). Even more astonishing is the range of temperatures (4–5200 K) achieved in various static and dynamic (shock-wave) pressure experiments.

One point we particularly wish to emphasize is the need for a good theoretical understanding to properly interpret and use experimental results. This is particularly true at ultra-high pressures, where strong crystal field effects can be misinterpreted as incipient insulator-metal transitions.

We have tried to point out apparatus, techniques, and results that we feel are particularly noteworthy. We have also included some of the "oral tradition" of high pressure Raman spectroscopy — useful little things that rarely or never appear in print. Because this field is rapidly expanding, we discuss a number of exciting new techniques that have been informally communicated to us, especially those that seem to open new possibilities.

THEORETICAL CONSIDERATIONS

Raman spectroscopy allows us to determine some (but usually not all) of the vibrational frequencies of molecules in crystals or fluids. The key points for our purposes are:**

1. The energies of vibrational modes are quantized.

2. The electric field **E** of light incident on the sample induces a dipole **p** according to

$$\mathbf{p} = \alpha \mathbf{E} \ ,$$

* This work performed under the auspices of the U.S. Department of Energy.

** Interestingly, one does not need much more than the barebones theory presented in these four points to get started. This makes Raman spectroscopy an excellent way to introduce new students to the high-pressure laboratory with publishable projects.

where α is the polarizability tensor of the sample.

3. If a particular vibrational mode modulates the polarizability then it can couple to the light incident on the sample.

4. The resultant coupling causes an incident monochromatic photon of energy $E = \hbar\omega_p$ to lose or gain an amount of energy $\hbar\Omega$ corresponding to a vibrational quantum.

More details of the interaction processes involved are discussed in the section on Raman Techniques below. To interpret Raman spectroscopy data, it is necessary to understand how the vibrational modes arise in a molecular crystal, a topic which is intimately entwined with elementary group theory.

The behavior of the molecular vibrational modes in a crystal depends on:

1. Molecular structure (molecular symmetry)
2. Local static environment (site symmetry)
3. Dynamical couplings (factor group)

We start with the isolated molecule, which can be naively considered to be a system of masses connected by springs. The standard techniques of classical mechanics can then be used to determine the equations of motion of the atoms.[1] The dynamical (or force constant) matrix is set up and solved and the solution yields the normal modes of vibration of the molecule. In a normal mode, all the atoms simultaneously reach their positions of maximum displacement and at some other time also simultaneously pass through their respective equilibrium positions. Each normal mode has a single well-defined frequency. The number and nature of normal modes depends on the molecular symmetry. For a molecule of N atoms, there are 3N-6 normal modes if it is non-linear and 3N-5 if it is linear (no rotation about the molecular axis). The frequencies of the normal modes may all be different; or some may be the same, either accidentally or because of symmetry-related degeneracy.

We cannot go much further without applying elementary group theory. We shall not go into detail here, however, since there are several excellent introductions to group theory as applied to molecular symmetry.[1-5] We will instead give a simple example, that of a water molecule. In Fig. 1, we show the symmetry operations that transform the atoms (in their equilibrium positions) of a water molecule back into themselves. These operations include mirror planes (denoted by σ_v) and a two-fold

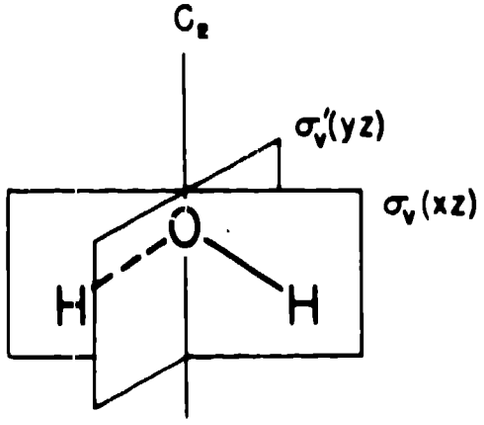

Fig. 1. Point group C_{2v} for H_2O. There are two mirror planes σ_v, and one two-fold rotation axis C_2.

Table I. Character table for point group C_{2v}.

C_{2v}	I	C_2	$\sigma_v(XZ)$	$\sigma'_v(yz)$			Optical Activity	
A_1	1	1	1	1	T_z	$\alpha_{xx}, \alpha_{yy}, \alpha_{zz}$	Raman	ir
A_2	1	1	-1	-1	R_z	α_{xy}	Raman	–
B_1	1	-1	1	-1	T_x;R_y	α_{xz}	Raman	ir
B_2	1	-1	-1	1	T_y;R_x	α_{yz}	Raman	ir

rotation (C_2). The list of all such symmetry operations makes up the point group, in this case C_{2v}.

When the atoms of the molecule vibrate, each normal mode breaks the symmetry of the molecule in a particular way. The character table for a point group indicates how the configuration associated with the displacements of each normal mode transforms under the symmetry operations of the point group. The displacements and frequencies for the normal modes must be calculated from the dynamical matrix; they cannot be determined from group theory. Group theory can, however, be used to determine the number of modes of each symmetry type, as well as whether these are Raman or infrared active or optically inactive.[3]

We continue with the example of water, as shown in Table I and Fig. 2. The number of normal modes in 3N-6 = 3 · 3 - 6 = 3. Comparison of the transformation properties listed in Table I and Fig. 2 shows that the ν_1 and ν_2 modes both have A_1 symmetry while ν_3 has B_1 symmetry.* All three modes are both Raman and infrared active.

Several other interesting facts about group theory are illustrated by this example. A particular molecule need not exhibit normal modes of all the possible symmetries permitted by its point group. In Table I the notation T_x, etc., in column 6 indicates the symmetry properties of translations along the x-axis, etc. Similarly R_x, etc., indicate the symmetry properties of rotations about the x-axis, etc. The components of the polarizability tensor α, which change during the vibration, are listed for each symmetry species in the seventh column. In order to be Raman-active, a normal mode must be associated with at least one of these components.[3] In order to be infrared-active, a normal mode must be associated with T_x, T_y, or T_z in column 6.[3]**

We shall be mainly concerned with linear molecules such as N_2, O_2, or CO, which belong to point groups $D_{\infty h}$ or $C_{\infty v}$. For historical reasons the notation for the symmetry elements for these point groups involves the use of capital Greek letters, which are also used for the electronic states of the same symmetry in homonuclear diatomic molecules. Hollas[2] gives character tables for $D_{\infty h}$ and $C_{\infty v}$ which relate the Greek letter notation to the Roman letter notation used for all the other point groups.

---

* The notation A_1, A_2, B_1, B_2, etc., to describe the symmetry properties is easy to understand and can be found in Hollas, Chapter 4 (Ref. 2), or Colthup, et al. p. 142, (Ref. 3). It is then necessary to understand what irreducible representations are all about. This is not hard either. (Colthup, p. 146, Ref. 3).

** This is because the dipole moment and displacement of the center of mass are vectors with the same transformation properties.

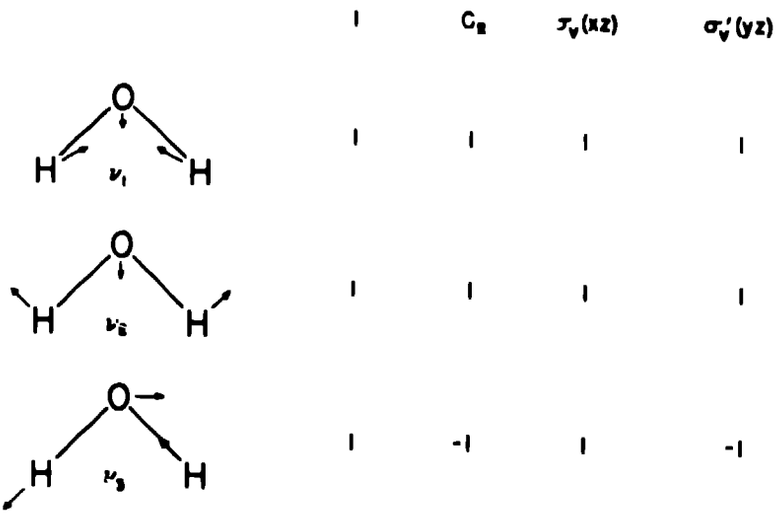

Fig. 2. The displacements for the normal modes of H_2O and their transformation properties under the point group C_{2v} symmetry operations, I, C_2, $\sigma_v(xz)$, $\sigma_v'(yz)$.

When the molecules assemble to form a crystal the situation becomes more complicated. The normal modes in a molecular crystal can be considered to be of two types:

1) internal modes, that is to say, the modes that are also present in the isolated molecule. These are often referred to as vibrons.

2) external modes, which are also called lattice modes, that involve relative motions of entire molecules. These can be subdivided further into librons (orientational motions) and phonons* (center-of-mass motions).

For most of what follows, we assume that the internal and external modes are in fact separable and that we are dealing with classical systems. We also assume that internal modes (vibrons) can be treated as perturbed free-molecule vibrations.

When a molecule is put in a lattice the (internal) modes change according to the symmetry of the environment. Group theory allows us to predict many aspects of these changes: how many new modes, the symmetry of these modes, whether they are Raman or infrared active. Group theory cannot predict the intensity of the spectra or the magnitude of splittings or shifts in the frequencies of the modes.

The changes in the modes depend on:[4,6]

(1) Site symmetry: the static crystal field of the site that the molecule inhabits. Here we treat the single molecule as vibrating in the mean field of surrounding rigid molecules.

(2) Factor Group: the dynamical, resonant, intermolecular vibrational couplings (vibrational excitons), which depend on the factor group of the crystal. The factor group is the space group without the translationnl symmetry, i.e., it is something like the point group of the unit cell and tells how parts of the cell are related to each other.[4] The splittings and shifts that arise from these

* This is the term used by chemists. There is some confusion when they talk to physicists who consider all the lattice vibrations in a crystal to be phonons.

resonant interactions are also called Davidov splittings or vibrational exciton splittings.[4,6]

We shall not go into detail here about how to calculate the correlation diagrams that tell how vibrations in the free molecule change with the site symmetry and factor group symmetry of the crystal. There are useful books that go into this in some detail.[7] Suffice it to say that it is really quite simple, and, if one follows the instructions carefully, is almost foolproof even for those who know little group theory. We shall talk about one example: a diatomic molecule in an ordered fcc structure. For this discussion, we neglect a number of subtleties such as overtones, hot bands, and couplings between modes. The analysis is made easier by the $\mathbf{k} = 0$ selection rule for Raman and infrared spectroscopy in a crystal. We should note that while the international symmetry notation for the symmetry of a space group of a crystal is generally more useful than the Schönflies notation, the latter is more useful in group theoretic analysis of vibrations since the factor group is the point group upon which the Schönflies notation is based.[4] For instance, the $Pa\bar{3}$ structure is given in Schönflies notation by T_h^6 and the factor group is just T_h.

Nitrogen in its low-temperature, low-pressure structure has four molecules per unit cell with the centers of mass in fcc positions and the orientations along the various body diagonals.[8] The structure has a $Pa\bar{3}$ space group (#205 in the International Tables for Crystallography[9]) and the x-ray determination gives the molecules in the 4a positions. From the International Tables, the site symmetry for the 4a positions is given as $\bar{3}$, which is S_6 in the Schönflies notation (there are tables that give the conversion between the two notations). As noted above, the space group in the Schönflies notation is T_h^6 so the factor group is T_h. In Table II we show the correlation diagram as constructed with the tables and procedures from the book by Fateley et al.[7] The basic procedure is as follows. First, find the correlation between the modes with their $D_{\infty h}$ symmetries and the site symmetry S_6. This step has the complication that the correlation tables do not have the $D_{\infty h}$ to S_6 correlation. However, we can see, for instance, that the internal vibrational mode of Σ_g^+ symmetry correlates to an A_{1g} mode in D_{6h} symmetry which then correlates to an A_g mode in S_6 symmetry. The same procedure can be followed for the rotations (R_x and R_y with Π_g symmetry) and translations (Σ_u^+ for translation along the bond T_z, and Π_u for translations perpendicular to the bond, T_x and T_y). We see that the modes are not split by the site symmetry. We follow the same procedure to see how the modes in the site are affected by the resonant interactions by finding the correlation between S_6 and the factor group T_h. The internal vibrational mode (vibron) is split by the factor-group interactions into two modes, a single A_g mode and a triply-degenerate F_g mode. Similar splittings are seen for the rotations (librons) and translations (phonons), with the number in parentheses indicating how many modes of that symmetry. The final step is to examine a character table for the factor group (T_h) and see what modes are Raman and infrared active, as discussed above for the water molecule. From this analysis we see that in solid nitrogen in its α structure there should be two Raman-active vibrons, three Raman-active librons, and three infrared-active phonons.

As we noted above, group theory is very useful in that it tells us about the number of modes, symmetries, and optical activities. It tells us nothing about the frequencies of the vibrations, the intensities of the transitions, or whether there may be accidental degeneracies. To understand these things, more complicated analyses that include the magnitudes of the interactions must be done. At zero temperature, for example, lattice dynamics calculations can be performed.[10] One can, however, obtain a sense of the physics by adopting a simple mean-field approach to calculate the shift in the vibron frequency due the static site potential and then allow for resonant couplings to give the factor-group splittings. For convenience, we will restrict our discussion to diatomic molecules.

Table II. Correlation diagram for α-N_2 Space Group $Pa\bar{3}$ (T_h^6).

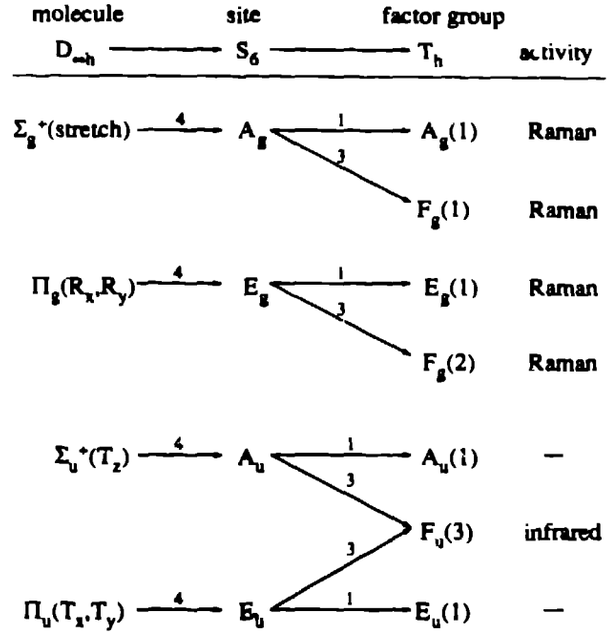

The interaction potential between two vibrating diatomic molecules i and j can be written as a Taylor expansion in powers of the bond length as[4,6]

$$V_{ij}(\vec{R}_{ij},\Omega_i,\Omega_j,r_i,r_j) = V_{ij}(\vec{R}_{ij},\Omega_i,\Omega_j,r_e,r_e) + \left(\frac{\partial V_{ij}}{\partial r_i}\right)_{r_e} r_i + \left(\frac{\partial V_{ij}}{\partial r_j}\right)_{r_e} r_j$$

$$+\frac{1}{2}\left(\frac{\partial^2 V_{ij}}{\partial r_i^2}\right)_{r_e} r_i^2 + \frac{1}{2}\left(\frac{\partial^2 V_{ij}}{\partial r_j^2}\right)_{r_e} r_j^2 + \left(\frac{\partial^2 V_{ij}}{\partial r_j \partial r_i}\right)_{r_e} r_i r_j + \cdots \quad ,$$

where $\vec{R}_{ij}$ is the vector connecting the centers of mass of the molecules, Ω_i and Ω_j are the orientations of the molecules, and r_i and r_j are the instantaneous bond lengths. The derivatives are evaluated at the equilibrium bond length, r_e, of the molecules. The terms of the form

$$\left(\frac{\partial V_{ij}}{\partial r_i}\right)_{r_e} r_i + \left(\frac{\partial V_{ij}}{\partial r_j}\right)_{r_e} r_j + \frac{1}{2}\left(\frac{\partial^2 V_{ij}}{\partial r_i^2}\right)_{r_e} r_i^2 + \frac{1}{2}\left(\frac{\partial^2 V_{ij}}{\partial r_j^2}\right)_{r_e} r_j^2 + \cdots$$

describe a field in which the molecules vibrate. Including these terms, appropriately averaged over all the molecules in the system, with the intramolecular vibrational potential

$$V_{\text{intra}} = \frac{1}{2}kr^2 + \frac{1}{2}gr^3 + \cdots \quad ,$$

where k and g are gas-phase force constants, gives a static-field vibrational potential from which a static, site-shifted bond length and frequency can be determined. If molecules in a crystal lie in different sites, then they will see different environments and may show distinct vibrational frequencies. The terms of the form

$$\left(\frac{\partial^2 V_{ij}}{\partial r_j \partial r_i}\right)_{r_e} r_i r_j + \cdots$$

describe the coupling between the vibrations on one molecule with those on another. These terms lead to resonant energy transfer (vibrational excitons) between

the molecules and the factor-group shifts and splittings. We will not go into detail here about how to calculate either the static-field site shifts or the dynamic factor-group splittings; those are well treated elsewhere.[4]

There are a couple of points that should be made before we leave theory and start the experimental techniques. First, group theory analysis can be very useful in distinguishing between possible structures on the basis of a Raman (or infrared or both) spectra. If the group theory states that a molecule in a certain crystal structure should show, for instance three phonon/libron lines and the spectra shows four, then the assumed structure is not likely to be correct. Later we shall discuss how such an analysis aided in the identification of a low-temperature structure in solid N_2 under pressure. Since the development of a correlation diagram is not difficult, there is no excuse for not doing it. The final point is that the factor-group shifts can be quite large, in fact as large or larger than the site shifts.[11] Since the factor-group shifts are due to resonant coupling between the molecules, they can be turned off by changing the fundamental frequency of the molecular vibrations through isotopic dilution studies.[4,6] The frequency shifts of a dilute H_2 molecule in D_2, for instance, would be due to the site shifts and would, to first order, contain no factor-group component. Thus, isotopic dilution studies can be very useful in distinguishing between the different types of interactions.

RAMAN TECHNIQUES

Spontaneous Raman Scattering (COORS)*

Spontaneous Raman Scattering (COORS) is the simplest Raman technique to understand as well as to use. It is also the least expensive to set up. COORS is described in detail in a number of standard references,[3,5] so we will not go into great detail. Fig. 3 shows a schematic view of the COORS process for a diatomic molecule.

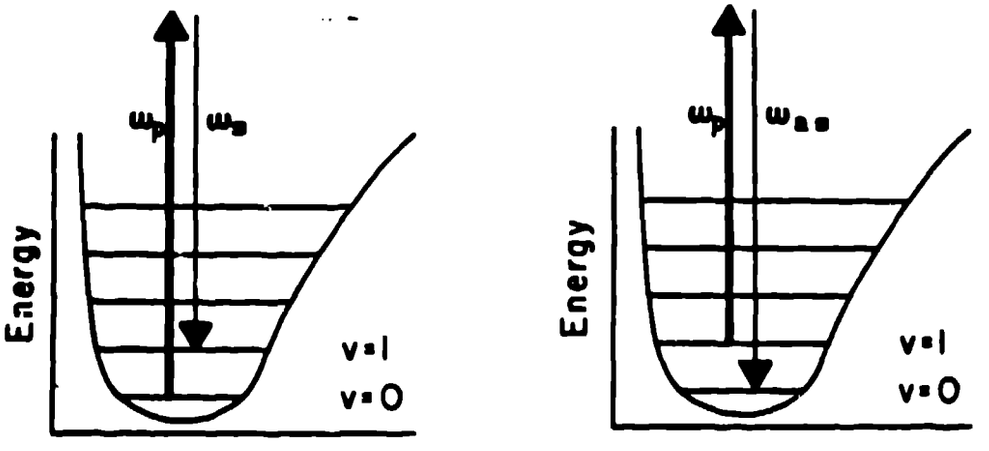

Fig. 3. COORS: The curve represents the vibrational potential energy function for a diatomic molecule (in the electronic ground state). The heavy arrows denote the incident laser energy. The light arrows denote the Raman-scattered radiation. The vibrational level quantum number is v. The left diagram represents the Stokes case, and the right one is for the Anti-Stokes case.

* Common Old Ordinary Raman Scattering, the acronym spells the name of a Colorado beer famous for the water in it.

If the Raman-scattered light loses energy it is called Stokes radiation and has angular frequency

$$\omega_s = \omega_p - \Omega \quad . \tag{1}$$

Raman-scattered light which gains energy is called anti-Stokes radiation with frequency

$$\omega_{as} = \omega_p + \Omega \quad . \tag{2}$$

The ratio of the anti-Stokes to Stokes intensities (away from an electronic resonance) is given by:[3]

$$\frac{I_{as}}{I_s} = \left(\frac{\omega_p + \Omega}{\omega_p - \Omega}\right)^4 \exp\left(-\hbar\Omega/kT\right) \tag{3}$$

where k is the Boltzmann constant and T is absolute temperature. At room temperature and below, usually only the $v = 0$ level is significantly populated, and only the Stokes line has significant intensity.*

In general, COORS signals are quite weak. However, they can be readily observed from samples in diamond-anvil cells and have even been observed in shock wave studies.[12] For static experiments, the sample is typically contained in a diamond-anvil cell with suitable apertures to allow the light to get in and out. Monochromatic light from an argon or krypton laser is passed through a plasma line filter and then focussed onto the sample with a short focal length objective. The COORS signal is collected with another objective and focussed onto the slits of a spectrometer. The signal is collected with a photomultiplier tube or Optical Multichannel Analyzer. Data collection is done automatically with a personal computer or the equivalent.

The first- and second-order COORS spectra and fluorescence of the diamond anvils can interfere with the COORS signal from the sample. The diamonds should be carefully selected for low fluorescence according to the prescriptions of Sharma and Adams.[13] The interference from COORS signals (as well as fluorescence) from the diamonds can be minimized by carefully designing the illumination and collection optics. The best design that we are aware of has been described by Hemley and coworkers.[14]

In the diamond-anvil cell, COORS can be performed over an extremely small area of the sample, typically 1–30 μm in diameter. This is important for studies at the highest pressures where the samples are small (~30–50 μm diameter) and the pressure gradients are large. For example, the pressure dependence of the vibron frequencies of nitrogen[15,16] and hydrogen[16] have been studied to over 170 GPa with COORS.

The COORS signals generally become weaker, broader, and harder to collect at very high (and more non-hydrostatic) pressures or very high temperatures. At low temperatures, they are more intense, especially the low frequency (Ω <450 cm^{-1})** modes.

The optics for collecting the signals from samples at high pressure and simultaneous very low or very high temperatures are constrained to be less than ideal. The fact that the diamond-anvil cell is in a cryostat or oven means that longer focal length

---

* COORS signals can sometimes be greatly enhanced by Resonance Raman Scattering (RRS). RRS takes place when the frequency ω_p of the laser is close to one of the electronic or vibrational transitions of the molecule. The resonance regions for the Stokes and anti-Stokes lines do not coincide. Thus, for a given ω_p, it is possible that the anti-Stokes line is much stronger than the Stokes line.[5]

** Conversion factors:
1 eV $\doteq 1.24 \times 10^{-4}$cm^{-1}
1 cm^{-1} = 10^{-7}/nm

lenses are required. Consequently, the laser spot is larger (~30 μm) and the COORS signal is less efficiently collected, both owing to the reduced f-number. Also, proportionally more fluorescence from the diamonds is collected due to the increased depth of field. The geometrical difficulties can be reduced by using very compact cells, such as the Merrill-Bassett[17] design. Their small size makes them easy to cool or heat as well. They have also proven to have impressive pressure capabilities ranging from[18] 30 GPa at 4 K to[19] 18 GPa at 900 K.

The COORS signal can also be improved by turning to an appropriate laser line, since the intensities go up as the laser frequency is increased. However, other choices of the laser line may greatly improve the ratio of the signal to the diamond fluorescence background for a particular vibration mode and set of diamond anvils. In some cases (for instance,[20] CO) yellow or red light is required to prevent photochemical reactions.

COORS has also been used in shock wave experiments, mostly on explosive molecules but also on water.[12] The small COORS cross-sections are particularly important in shock-compressed materials where the thermal radiation background may be large. The intensities may be improved by using ultraviolet lasers, although this increases the risk of inducing backgrounds due to fluorescence or photochemically produced species.[21]

Stimulated Raman Scattering

Stimulated Raman scattering is a coherent scattering process that occurs when the incident laser intensity exceeds a threshold and generates a strong directional (forwards and backwards) beam at the Stokes frequency.[21] A large fraction of pump intensity can be converted.[22] Stimulated Raman scattering has not been, to our knowledge, used in diamond-anvil cells, but was the first coherent Raman technique to be used in shock-compressed samples.[23] This technique has several major disadvantages which keep it from general use in either static or dynamic experiments: large incident laser powers are required and not all molecules have cross-sections large enough and line widths narrow enough. Only the lowest threshold transition in the condensed sample produces a signal.[21]

Coherent Anti-Stokes Raman Spectroscopy (CARS)

Coherent Anti-Stokes Raman Spectroscopy (CARS) is the most important of the coherent Raman techniques for studies on simple molecular materials at high pressure. The chief advantage of CARS is that is provides strong signals* with little interference from backgrounds due to fluorescence or thermal radiation. Compared to COORS, CARS is much more difficult and expensive to perform, but when large signal strengths or short data collection times (as in shock wave experiments) are crucial, it is the preferred method. CARS has been extensively used in shock wave studies, and is beginning to be used in diamond-anvil cells now. Already the Raman spectra at the highest temperatures[24,25] as well as at the highest pressures[26] have been obtained with CARS.

The theory of CARS is described by a number of authors.[22,27,28] We give only an outline of the process here, much of which is derived from the excellent article by Tolles, et al.[27] Two high-intensity pulsed laser beams with angular frequencies ω_p and ω_s are focussed together in the sample. As discussed below, non-linear effects due to the strong fields cause mixing of these frequencies to generate photons of angular frequency

$$\omega_{as} = 2\omega_p - \omega_s \quad . \tag{4}$$

* Up to 10^5 times those available with COORS.

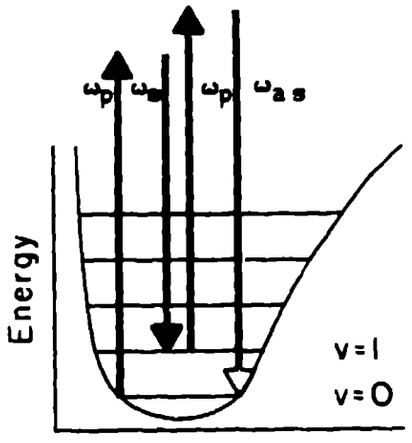

Fig. 4. CARS: The curve represents the vibrational potential energy level diagram for a diatomic molecule in the electronic ground state. The symbols have the same meaning as their counterparts in Fig. 3. The wide arrow (ω_{as}) denotes the coherent anti-Stokes emission.

These are emitted coherently as a well-defined beam.*

This process always produces a signal even in the absence of vibration modes. However, the efficiency of conversion drastically improves when the difference $\omega_p - \omega_s \rightarrow \Omega$ where Ω is a molecular vibration frequency. The pumping process is schematically illustrated in Fig. 4. Experimentally, the difference $\omega_p - \omega_s$ is swept, usually by varying ω_s; the output intensity $I(\omega_{as})$ is the CARS spectrum.

In contrast to the other forms of Raman scattering discussed above, CARS has the further complication that the propagation vectors $\mathbf{k}_s$ and $\mathbf{k}_p$ must be carefully aligned to get any resonance signal at all. The magnitude $|\mathbf{k}_i| = \omega_i n_i/c$, where ω_i is an angular frequency n_i is the refractive index and c is the velocity of light. Because of dispersion in the sample $n_p \neq n_s \neq n_{as}$. The four waves must satisfy momentum conservation as shown in Fig. 5.**

In high-pressure experiments, however, the indices of refraction are largely unknown. The angle θ between $\mathbf{k}_p$ and $\mathbf{k}_s$ must then be varied until sweeping $\omega_p - \omega_s$ produces the desired resonance. A tunable dye laser can be used to vary w_s, according to the scheme shown in Fig. 6. Alternatively, a broad-band dye laser may be used as depicted in Fig. 7. In this case, only the correct value of ω_s for resonance is picked out of the broad band.

In shock-wave experiments, the broad-band dye laser is used so that the tuning to resonance is essentially automatic.*** In static experiments, however, the tunable

---

* Other combinations such as $3\omega_p \rightarrow \omega_3$, $2\omega_p + \omega_s \rightarrow \omega_3$, etc., are also created, but these are not important for CARS.

** Calculations of the conversion efficiency for focussed beams depend critically on the nature of the beam profiles. Even the qualitative results can be quite different.[27]

*** The problem of determining the angle θ is overcome by using "sloppy" beams, containing the TEM_{01} (doughnut) mode as well as the gaussian TEM_{00}. The output intensity is about 20% of that expected for an optimal setup.

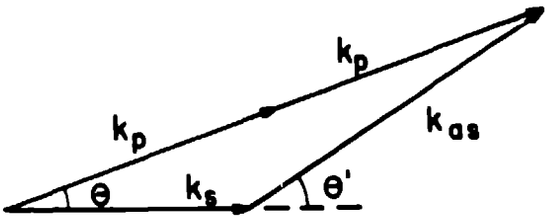

Fig. 5. CARS: Momentum conservation diagram.

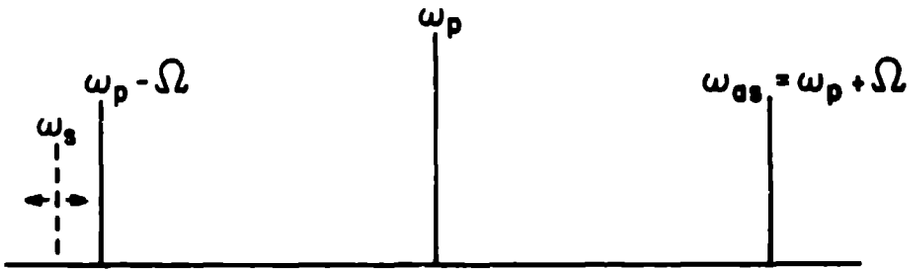

Fig. 6. CARS: using a tunable dye laser. The frequency ω_s is varied until it matches the resonance conditions $\omega_s = \omega_p - \Omega$.

dye laser has the advantage of much greater intensity at the value of ω_s.

The analysis of CARS data, even at the simplest level, is considerably more complicated than for COORS. To begin with, curve-fitting is generally required to obtain the value of Ω from the raw CARS data. The peaks in a CARS spectrum are not centered on $\omega_p + \Omega$ as in anti-Stokes COORS, but are shifted. It is necessary to discuss some further details of the CARS process to show the main causes of the peak shapes. We begin by expanding the polarization **P** of the sample in a power series in the electric field strength **E**:[27]

$$\mathbf{P} = \chi_1 \mathbf{E} + \chi_2 \mathbf{E}^2 + \chi_3 \mathbf{E}^3 + \quad , \tag{5}$$

where the χ_i are the electric susceptibility coefficients. Only χ_3 concerns us here because the CARS intensity I_{AS} is proportional to $|\chi_3|^2$. In general χ_3 is a tensor of rank four, but we can treat it as a scalar if all the E-fields are parallel.

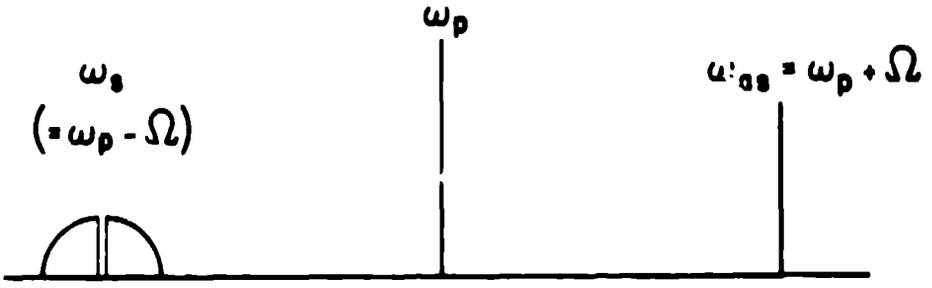

Fig. 7. CARS: with a broad-band dye laser.

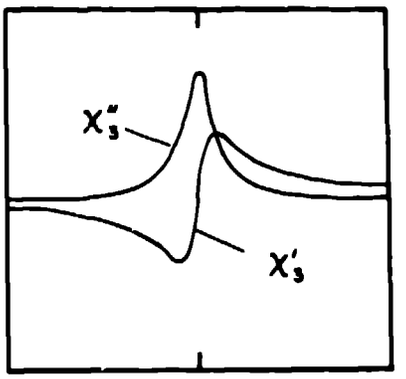

Fig. 8. Behavior of χ_3' and χ_3'', the dispersive and absorptive parts of χ_3^{res}, respectively.

The effect of an intense E-field on matter is to polarize it non-linearly. For this reason, even in substances without vibrational resonances χ_3 is real and positive. When vibrational levels are present, the conversion efficiency increases greatly as $\omega_p - \omega_s \rightarrow \Omega$ due to changes in the susceptibility. The susceptibility is therefore usually written as

$$\chi_3 = \chi_3^{res} + \chi_3^{NR} \quad , \tag{6}$$

where χ_3^{res} is the contribution to χ_3 from a resonance and χ_3^{NR} is the non-resonant contribution. In the vicinity of a resonance,[27,29]

$$\chi_3^{res}(\omega) \sim \left[\frac{\chi_3^{Pk}}{(\Omega - \omega_p + \omega_s) - i\Gamma}\right] \tag{7}$$

where χ_3^{Pk} is the peak third order susceptibility and Γ is the half width at half maximum. Thus, $\chi_3^{res}(\omega)$ is a complex quantity which can be written as

$$\chi_3^{res}(\omega) = \chi_3' + i\chi_3'' \quad , \tag{8}$$

where $\chi_3'(\omega)$ and χ_3'' are the dispersive and absorptive parts of $\chi_3^{res}(\omega)$, respectively.

Then CARS intensity is therefore

$$\begin{aligned} I_{AS}^{(\omega)} &\sim |\, \chi_3(\omega)\,|^2 \\ &\sim |\, \chi_3'(\omega) + i\chi_3''(\omega) + \chi_3^{NR}\,|^2 \\ &\sim \left(\chi_3'\right)^2 + 2\chi_3'\chi_3^{NR} + \left(\chi_3^{NR}\right)^2 + (\chi'')^2 \quad . \end{aligned} \tag{9}$$

The behavior of χ_3' and χ_3'', the dispersive and absorptive parts of χ_3^{res}, are shown in Fig. 8. Because χ_3' swings from negative to positive at resonance, the crossterm $\chi_3'\chi_3^{NR}$ in Eq. (9) introduces a strong asymmetry in I_{AS}. This is why the CARS peaks are shifted from the positions found in COGRS. Actual data analysis is even more complicated because it is necessary to deconvolute the profile of the laser intensity as a function of frequency and also to consider the spectral response of the detection system.

The raw CARS spectrum for benzene at P = 10.6 GPa and T $\approx$ 1200 K is shown in Fig. 9, along with the intensity profile of the broadband dye laser. The effects of the $\chi_3'\chi^{NR}$ cross-term and the intensity profile of the dye laser can clearly be seen.

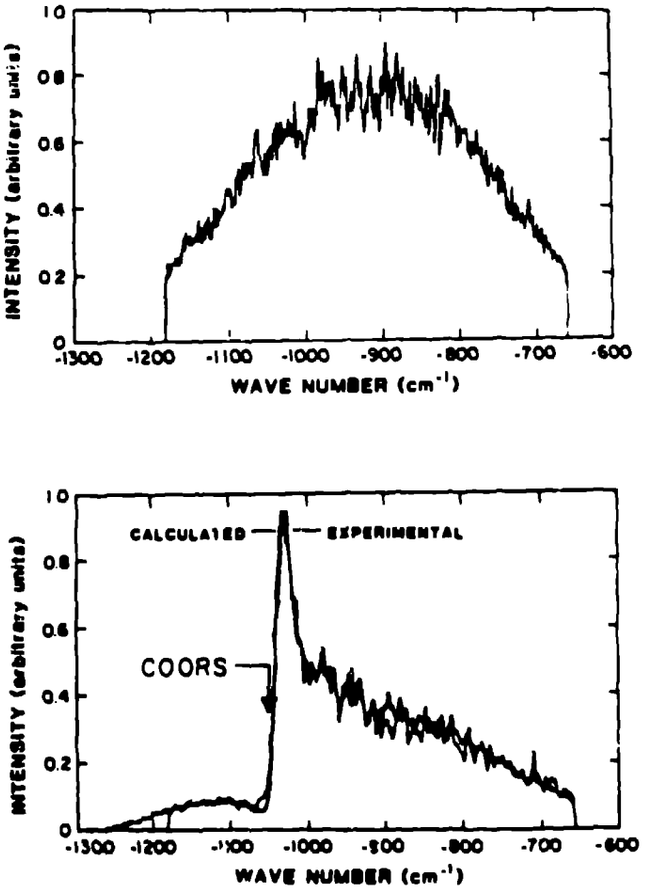

Fig. 9. CARS spectrum for shock-compressed benzene at 10.6 GPa.[29] Upper spectrum is the broadband dye laser spectral profile. Lower spectrum is CARS peak convoluted with the broadband profile. The approximate position of the corresponding COORS peak is denoted by the arrow.

Impulse-Stimulated Scattering

Impulse-Stimulated Raman and Brillouin Scattering (ISRS and ISBS, respectively) are two very new and promising spectroscopic techniques which should be especially useful in high-temperature diamond-anvil cells.[30] The two techniques are essentially the same, differing only in timescales. To date, the most emphasis at high pressure has been on ISBS, which we shall discuss here, though some ISRS spectroscopy has been done.[31]

In ISBS, a pulsed (~30 ps) laser beam is split into two beams which are simultaneously brought into a sample at a fixed, well-determined angle θ, as shown in Fig. 10. The two "excitation" beams are "focused" to a fairly large spot about 200 μm in diameter. Because the two beams have a fixed phase relation, interference fringes form. These interference fringes induce a standing acoustic wave in the sample because local heating or electrostriction* is greatest at the electric field maxima. This standing acoustic wave can serve as an acoustic grating in the sample, from which another, time-delayed, laser pulse can be scattered. By measuring the amplitude of the scattering of this secondary probe pulse as a function of time delay after the ex

* These are distinctly different effects.

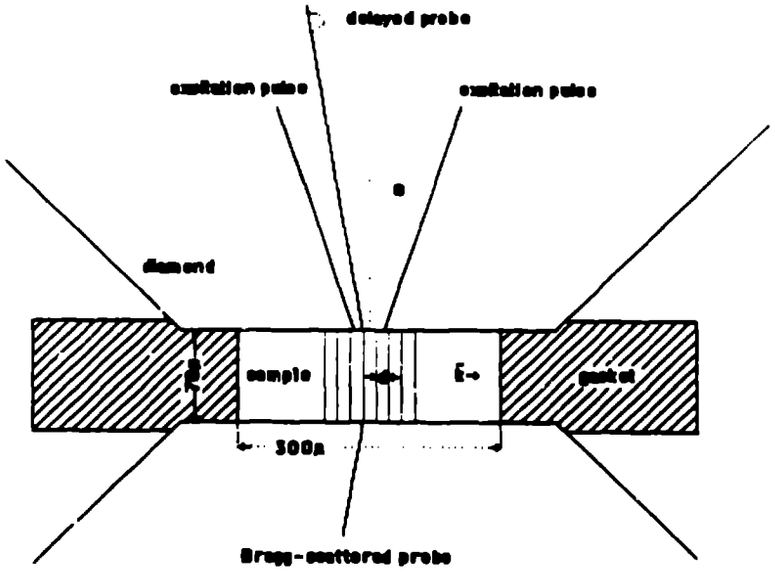

Fig. 10. Schematic view of ISBS in a diamond-anvil cell.

citation pulses are turned off, the frequency and wavelength of the standing wave can be determined, from which the sound velocity can be calculated. In Fig. 11, results from a recent study on methanol are shown at ambient pressure and at 3 GPa.[32] The increase in sound velocity with pressure is apparent from that figure. From the relation of sound velocity to pressure, the equations of state of methanol and ethanol were determined.

There are a number of advantages to the use of ISBS over normal Brillouin scattering techniques. First, because the wavelength of the excitation pulses and the angle between them are known, the index of refraction is not needed. Second, the problem of having a very weak signal near a strong laser pulse is not present, eliminating the need for fancy signal processing.

APPLICATIONS

Raman spectroscopy has been performed on a large number of simple molecular substances at high pressures, including H_2,[16,26] N_2,[15,16,19] O_2,[33] F_2,[34] Cl_2,[35] Br_2,[36-38] I_2,[39] CO,[20] CO_2,[40,41] N_2O,[42] N_2O_4,[43] N_2O_3,[42,43] CS_2,[37,44] SO_2,[45] CH_4,[46] NH_3,[47] H_2O,[12] H_2S,[48] HCl,[49] HBr,[50] and HI.[51] We will discuss, however, Raman spectroscopy on only two molecular materials at high pressures, nitrogen and hydrogen, and only nitrogen in detail. Nitrogen and hydrogen provide examples of most of the kinds of spectroscopic information available. Nitrogen was the earliest of these materials to be studied with Raman spectroscopy in a diamond-anvil cell[52] and has now been studied over a greater area of P-T space than any other molecular material. The Raman studies on N_2 illustrate the power of the technique for determining phase diagrams and even (up to a point) crystal structures and molecular ordering. The Raman data for N_2 also provides a clear case for the need of a careful theoretical treatments of the relation between the pressure dependence of the vibron frequencies and changes in bond strengths and possible insulator-metal transitions. This is crucial for using the N_2 vibron shift as a spectroscopic pressure scale at high temperatures. We shall discuss (briefly) some recent results on hydrogen at high pressures in light of its possible insulator-metal transition.

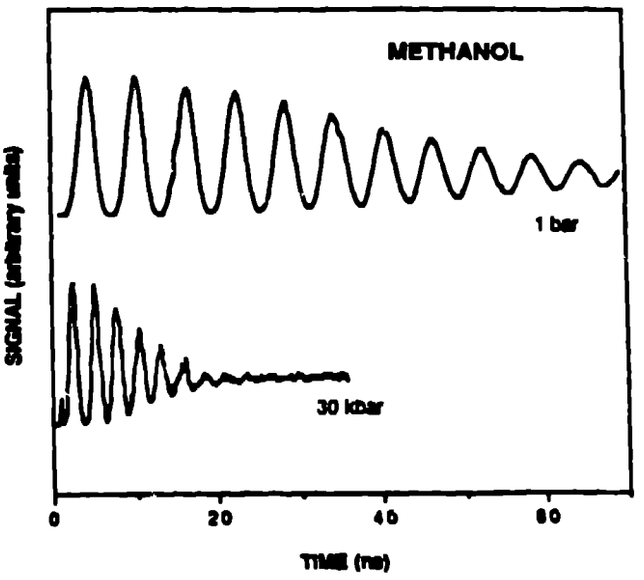

Fig. 11. Time-domain diffraction data for methanol in a diamond-anvil cell at room temperature.[32]

Nitrogen

At room temperature above about 2.3 GPa, N_2 freezes into the $\beta - N_2$ (cph) structure,[53] whose Raman spectrum consists of a single vibron peak. Above 4.5 GPa, the appearance of two well-separated vibrons is the first hint that the Raman spectra of N_2 at high pressures is complex and interesting.[52] Single-crystal x-ray diffraction structure determinations show that N_2 at this pressure has a new cubic structure: $\delta - N_2$ with space group Pm3n.[54] In this structure, which is essentially the A15 structure,* the N_2 molecules are located at two distinct symmetry sites and exhibit two distinct types of disorder, as shown in Fig. 12. The ν_1 vibrons are from the spherically disordered molecules and the ν_2 vibrons are from the pancake disordered molecules. As determined by Raman spectroscopy, the $\delta - N_2$ (Pm3n) structure is stable in the vicinity of the melting curve up to at least 18 GPa and 900 K.[19]

The A15 structure is known to distort into a variety of lower symmetry structures with suitable small changes in P,T conditions. In the case of N_2 the distortions can occur as the molecules of δ-N_2 become ordered either at very low temperatures or much higher pressures. The study of these phase transitions with Raman spectroscopy demonstrates the power of this technique.

We start with the behavior of nitrogen at about 15 K. Above 2 GPa, a pair of vibrons appear just as in the case of δ-N_2. However, seven external modes of lower frequencies also appear. The Raman spectra, along with theoretical structural calculations and a few reasonable assumptions, were enough to predict that this low-temperature distortion (now called ε-N_2) of the δ-N_2 (Pm3n) structure almost certainly had space group R$\bar{3}$c.

---

* The A15 is the structure of the old "high temperature" superconductors, such as Nb_3Ge. The pancake disordered molecules are on the Nb sites and the spherically disordered molecules are on the Ge sites. $\delta - N_2$ is transparent and is not a conductor let alone a super-conductor.

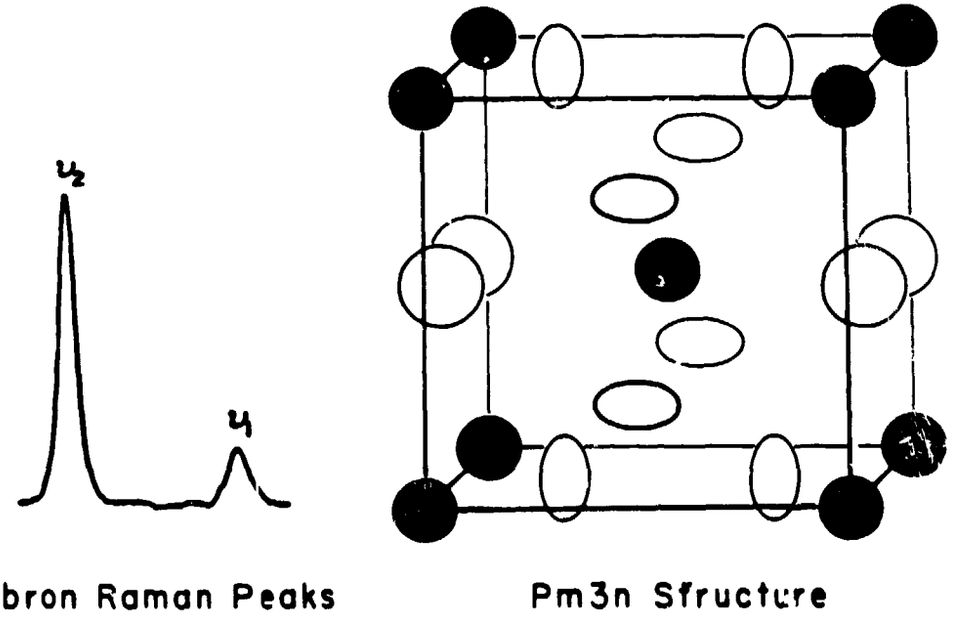

Fig. 12. δ-N_2 at 424 K and 18.4 GPa. The Pm3n structure has N_2 molecules with two distinct types of disorder at different site symmetries. The ν_1 vibrons are from the spherically disordered molecules at the body-centered positions (dark circles), and the ν_2 vibrons are from the pancake disordered molecules on the faces (open symbols).

In the original work,[55] the correlation diagrams of the Pm3n cubic structure of δ-N_2 as well as cubic, rhombohedral, tetragonal, and orthorhombic distortions were considered. For each distortion the centers of the molecules were located at sites with symmetries that were subgroups of the 6c(D_2) and 2a(T_h) site symmetries in δ-N_2.[9] Only structures with the same number of molecules per unit cell were considered; superlattices were excluded.* We are interested in the highest symmetry structures consistent with the Raman data. Of course, depending on the magnitude of the distortions, any lower symmetry structure may also be a possibility.

The high-symmetry space groups to consider are: Pm3n, Pm3, (cubic) R$\bar{3}$c, $P4_2/mmc$. Lower symmetry structures allow so many external modes that they appear consistent with any data, in the absence of line intensity calculations. Space group Pm3n can account for only four of the seven external modes, and can therefore be ruled out.** Space group Pm3 can allow nine external modes, but the ν_1 peak should split because it arises from two different sites 1a (T_h) and 1b (T_h). The fact that the ν_1 peak is not split does not conclusively rule out Pm3, but it should make us very suspicious. $P4_2/mmc$ can be ruled out because the symmetry requires inefficient packing.

The R$\bar{3}$c structure may have eight Raman-active external modes. No other space group comes as close to the observed seven. The vibrons should be indistinguishable from those in δ-N_2 (Pm3n), as observed. Theoretical calculations[56] also

* This assumption turns out to be appropriate here, but is probably not correct for the distortions occurring at very high pressures at 300 K.

** Group theory for site 6c (D_{2d} of Pm3n) also predicts two ν_2 peaks instead of the one that is actually observed. This is not a difficult problem. Either of the peaks could be extremely weak, or the two may be unresolvable. This situation persists for all the subgroups of D_{2d} encountered in the possible distortions of the δ-N_2 structure.

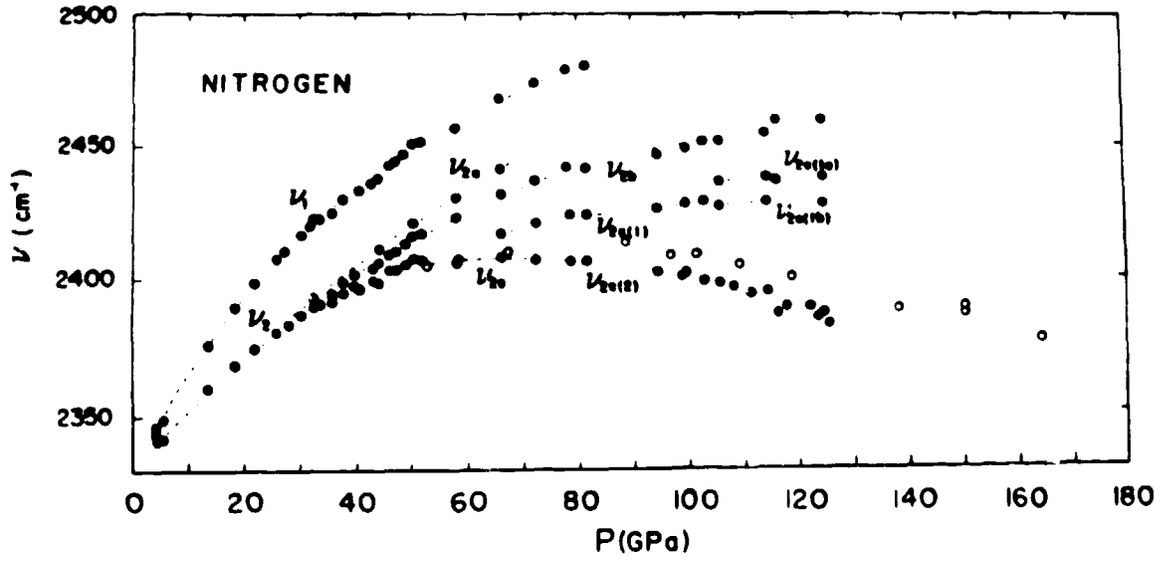

Fig. 13. Nitrogen vibron spectrum at high pressure and room temperature. Solid circles from Ref. 15, and open circles from Ref. 16. The original ruby pressure scales used respectively by the authors are reported here without alteration, although it is clear that some reconciliation is required.

indicated that R$\bar{3}$c was the most stable structure for N_2 at 2 GPa. For these reasons R$\bar{3}$c was the favored structure.* It should be noted that the structure could be determined this well with Raman data because it was closely related to a known structure and because theoretical structure calculations strongly favored it. The need for close experimental and theoretical collaboration is a theme that arises again and again with nitrogen, as well as with hydrogen.

Further increases in pressure at 15 K cause another interesting transition starting at about 21 GPa. The ν_2 vibron splits, while the external modes are only weakly affected. The new structure is unquestionably a small distortion of ε-N_2 (R3c), probably rhombohedral. Here theoretical calculations could not give a new stable structure, and while space group R$\bar{3}$c is the best choice consistent with the splitting of ν_2, it is by no means conclusive. It is interesting to note that the crystal fields can induce such a large splitting in the ν_2 vibron while the external modes are only moderately perturbed.

We turn now to the Raman spectra of solid N_2 at the highest pressures yet attained, as shown in Fig. 13. At about 20, 65, and 105 GPa three new transitions take place. These can be discerned by splittings or changes in the shapes of the Raman-active vibron peaks. While the new structures are not yet known completely, they are most likely distortions of the δ-N_2 (Pm3n) structure and they are clearly different from the low-temperature distortions discussed above.

A feature that has stirred considerable speculation is the broad maximum in the range 60-80 GPa in the lowest frequency vibron. What is the cause of this maximum? It is certainly possible that this maximum may be associated with the eventual dissociation of the N_2 bond. Theoretical calculations have estimated the pressure necessary for such a dissociation to be under 80 GPa.[58] The shift in the absorption spectrum,[59] which is accompanied by dramatic color changes, to pinkish brown and finally very dark brown, is consistent with major changes in the electronic structure and thus with a weakening of the diatomic bond. Moreover, shock-wave experiments have shown a softening of the compressibility above 40 GPa (and much

* This was subsequently confirmed by x-ray powder diffraction.[57]

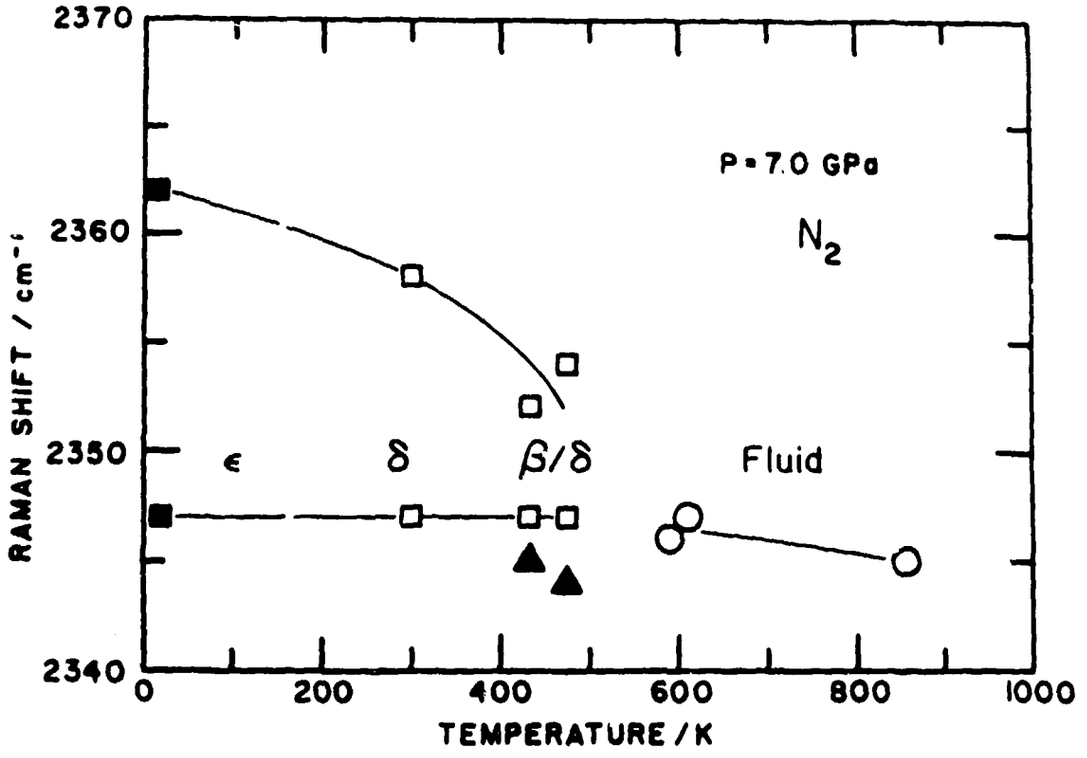

Fig. 14. Nitrogen vibron frequencies at constant pressure (7 GPa) as a function of temperature. Solid squares are ε-N_2, open squares are δ-N_2, solid triangles are β-N_2, and open circles are fluid-N_2.

higher temperatures).[60] On the other hand, the downturn may be due only to strong factor group interactions. First of all, the downturn accompanies a structural transition and only affects a single mode. It is reasonable to assume* that the same molecules participate in several of the Raman-active vibrons. In that case, we cannot argue that a decrease in the frequency of only one mode is due to a weakening of the molecular bond.

Fortunately, the question can be decided experimentally with samples containing a few percent $^{15}N_2$ in $^{14}N_2$. If the maximum in the lowest frequency vibron is due to a bond weakening, the $^{15}N_2$ impurity modes will show the same qualitative behavior as shown in Fig. 13. If the maximum is due to strong factor-group interactions, then the corresponding vibron frequency for $^{15}N_2$ molecules will simply continue to increase because they are not resonantly coupled to the $^{14}N_2$ molecules.

The behavior of the vibrons in N_2 as a function of temperature at high pressure turns out to be very interesting and useful. The vibron in the fluid, as well as the ν_2 vibron in δ-N_2 and its distortions, provides the basis for a spectroscopic high-pressure scale which should be applicable from the lowest attainable temperatures to many thousands of degrees Kelvin. Both experiment[19,24,25] and theory[61,62] show that there is surprisingly little temperature dependence in the vibrons. In addition,

* Because we do not know the crystal structures, we are also ignorant of the number of Raman-active vibronic modes each molecule contributes to. That depends on the number of independent symmetry sites that exist in the rather complicated new structures. It is conceivable that the molecule associated with a particular site symmetry forms conducting chains or clusters, although we do not think this is likely in nitrogen.

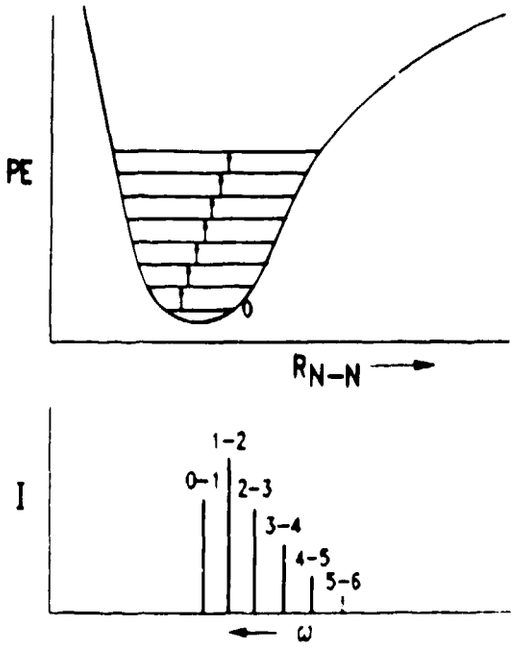

Fig. 15. Population distribution in an anharmonic potential at high temperatures.

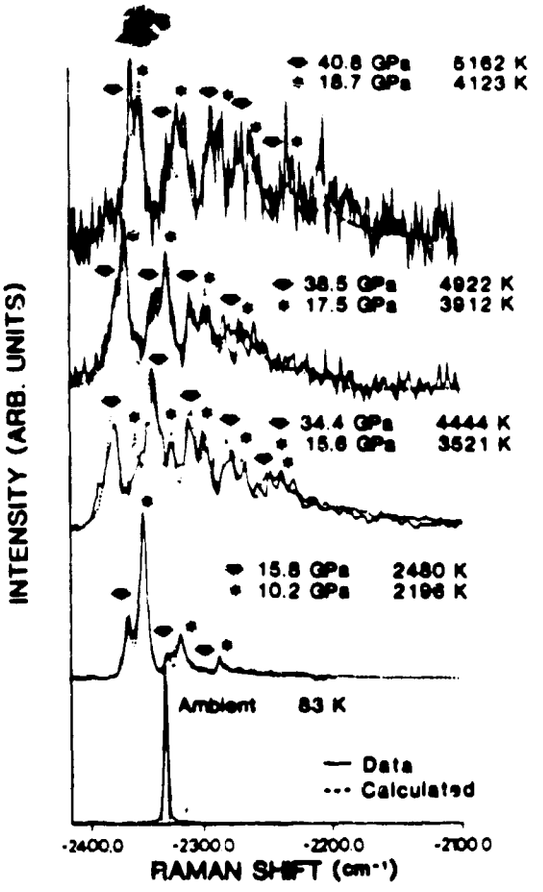

Fig. 16. Vibron in shocked fluid nitrogen.[25]

comparison of the ν_2 and fluid frequencies gives a tantalizing hint about the nature of the orientational order to be found in the fluid along the melting curve.

The vibron frequencies of N_2 as a function of temperature at a constant pressure of about 7 GPa are shown in Fig. 14. There are a number of interesting features in this figure. First, the peaks associated with molecules in the β-N_2 structure are clearly shifted from the other solid structures. The difference in frequencies is a measure of the different environments the vibrating molecules feel in the two structures. Also, while the higher frequency ν_1 vibron in ϵ- and δ-N_2 is strongly temperature dependent, the lower frequency ν_2 vibron is essentially independent of temperature, a behavior which persists in the fluid as well. Indeed, there is almost no discontinuity between the ν_2 vibron in the solid and that in the fluid. Since there is a large change between the ν_1 vibron and the fluid, the data imply that the environment of molecules in the pancake-disordered sites (ν_2) is more similar to that in the fluid than that of the molecules in the spherically-disordered sites (ν_1). Since the environment depends on the local structure, these data indicate that the local structure in the fluid may be more similar to the local structure around the pancake-disordered molecules than that around the sperically-disordered molecules. Recent Monte Carlo calculations[62] support this view. Comparison of the pair distribution functions for the fluid and the δ-N_2 solid show indeed that the structure of the fluid is much more akin to that around the pancake-disordered molecules. The physics of this phenomena is clear. To minimize repulsion between the molecules in the fluid,

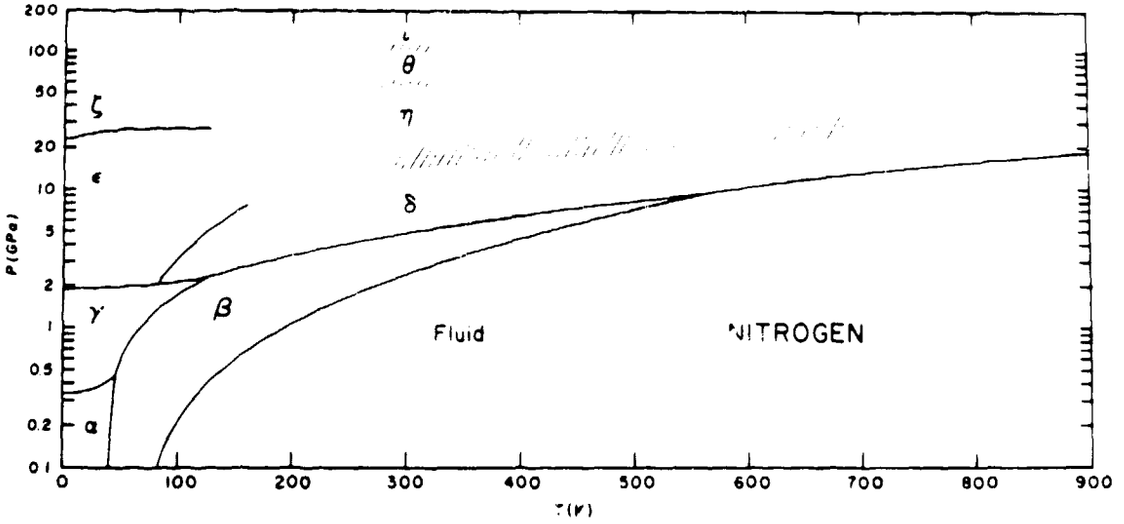

Fig. 17. Phase diagram of nitrogen, determined mostly with Raman spectroscopy.

they line up in a parallel fashion, as do the molecules along the faces of the δ-N_2 structure (Fig. 12).

The use of shock-wave techniques opens the door to the study of materials at very high temperatures. Recent work using CARS to study shocked nitrogen reached temperatures of over 4000 K. The temperature was sufficiently high that vibrational levels other than the ground state were populated. In Fig. 15 we show a typical example of the population distribution in an anharmonic potential at very high temperatures. The data from the CARS experiment is shown in Fig. 16. The experimental spectra are complicated by the presence of signal from both singly-shocked and doubly-shocked samples. Comparison of the temperature derived from an analysis of the population distribution with that derived from an equation of state indicates that the vibrons are in thermal equilibrium with the other modes in the system. The splittings between the different transitions (0-1, 1-2 etc.) provide evidence that the overall anharmonic shape of the intramolecular potential does not change much in shocked nitrogen.

We end our discussion of N_2 with the phase diagram shown in Fig. 17, which was determined almost entirely with Raman spectroscopy. At relatively low pressures and temperatures, the structures were determined by X-ray diffraction.[8,53,54,57] However, once the structures of ε-N_2 and δ-N_2 were determined, Raman spectroscopy allows us to describe the structure of ζ-, η-, θ-, and ι-N_2 as distortions of these.[15,52,55] The melting curve has been followed further for N_2 than for any other molecular substance.[19] Not all other molecular materials are as convenient for study with Raman spectroscopy as nitrogen; however, the case of N_2 shows what can be achieved.

Hydrogen

The vibron ($Q_1(1)$) band of pure hydrogen has been followed up to about 150 GPa with COORS[16] and 200 GPa with CARS,[26] as shown in Fig. 18. The most dramatic feature of Fig. 18 is the broad maximum in frequency seen in H_2 at about 30-40 GPa and in D_2 at about 60-80 GPa. In pure H_2, by 200 GPa the frequency of the vibron has dropped by about 30% relative to the gas-phase value. Many have speculated that this downturn is an indication of a softening of the hydrogen bond prior to a predicted metal-insulator transition.[6,63] Infrared spectra up to 54 GPa, however,[64] show several bands that increase in frequency with pressure. One

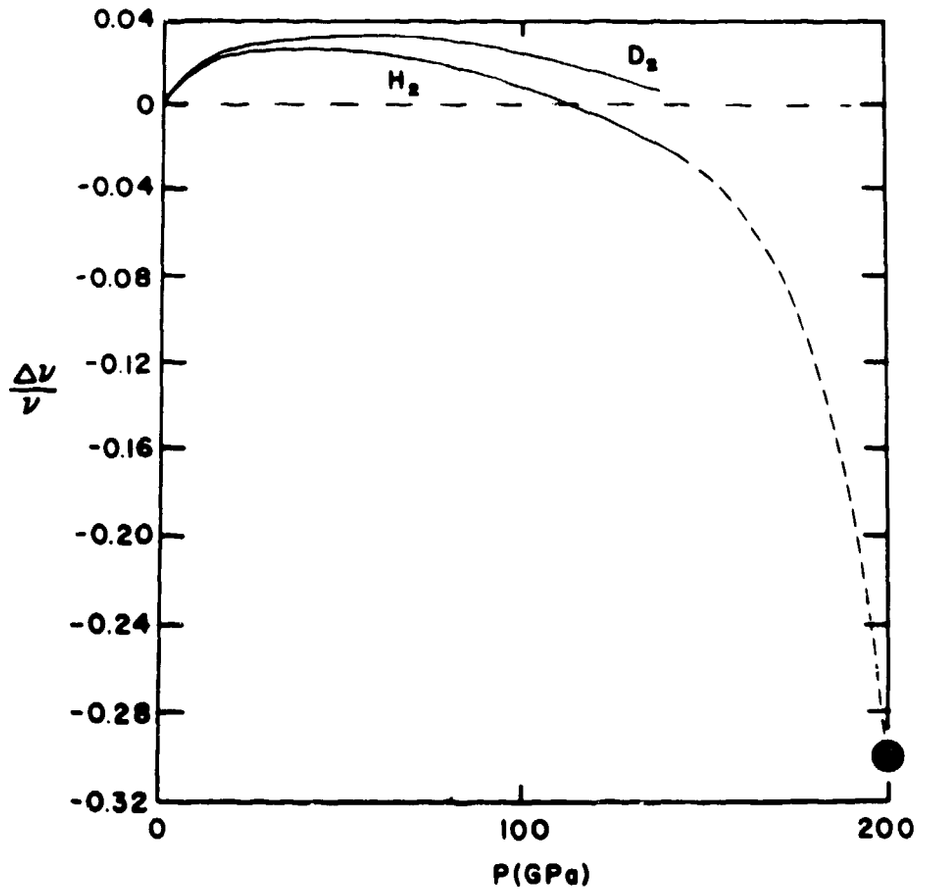

Fig 18. Raman frequency shift $\Delta\nu/\nu$, where ν is the unperturbed frequency, of the hydrogen vibron as a function of pressure. Solid lines are COORS data from Bell et al (Ref. 16) and the solid circle is from a recent CARS experiment by Yu et al (Ref. 26). The dashed line is a freely drawn interpolation between the two sets of data.

band, identified as the $Q_1(1)$ band,* may show some signs of leveling off by 54 GPa, but there is no indication of the sharp downturn seen in the Raman spectra. As for nitrogen, the question then arises whether the downturn is due to a change in bond strength or, rather, to resonant interactions. Recent studies by Daniels and coworkers[65] using isotopically dilute H_2 in D_2 and D_2 in H_2 indicate that the lowntum is due to resonant interactions. As would be predicted from an analysis including the resonant interactions,[6] the vibron peak associated with an isotopically-dilute molecule tracks with the infrared transition which, in the case of an hcp lattice, is the band center. Thus, the downturn does not indicate incipient bond weakening, but rather is due to dynamic couplings between molecules.

SUMMARY

We have tried to give a concise summary of some of the aspects that we feel are important for Raman spectroscopy on simple molecular systems at high densities. We certainly could not go into great detail about any aspect of the use of Raman spectroscopy; we hope, however, that we provided enough of a guide that someone could get started to use this very important tool.

---

* This transition corresponds to the pure vibron and would normally not be infrared allowed (no dipole moment in an H_2 molecule). Collisionally-induced dipoles are responsible for its infrared signal.[6]

There are a number of points that we would like to emphasize. First, because Raman spectroscopy is relatively easy to use in a diamond-anvil cell, it is perhaps the most important technique for molecular systems at high pressures. While Raman spectra cannot answer all questions about the structure and properties of a molecular system, there is much physics associated with the shifts in frequencies observed at high pressures. As was discussed, the intermolecular interactions lead to the frequency shifts and, indeed, these shifts provide a microscopic measure of the forces between molecules. However, Raman data cannot be used reliably by itself; supporting information from theory or other experiments is necessary to fully interpret the data. Since Raman data is often the only data available at high densities, we urge theorists to compare, as much as possible, theoretically predicted frequency shifts with experimental data.

ACKNOWLEDGEMENTS

We would like to thank Mike Brown, L.-T. Chang, K. A. Nelson, and L. J. Slutsky for sharing their work prior to publication and for permission to print Figures 10 and 11. We would also like to thank Bill Daniels and coworkers, Russ Hemley, and Robin Reichlin for sharing their work with us prior to publication and Malcolm Nicol for many helpful discussions. This work was partially supported by a grant from the Division of Materials Science of the Office of Basic Energy Sciences of the U.S. Department of Energy.

REFERENCES

1. E. B. Wilson, Jr., J. C. Decius, P. C. Cross, "Molecular Vibrations," McGraw-Hill, New York (1955).

2. J. M. Hollas, "Symmetry in Molecules," Chapman and Hall, London, UK (1972).

3 N. B. Colthup, L. H. Daly, and S. E. Wiberley, "Introduction to Infrared and Raman Spectroscopy," Academic Press, New York (1975).

4. J. C. Decius and R. M. Hexter, "Molecular Vibrations in Crystals," McGraw-Hill, New York (1977).

5. M. M. Sushchinskii, "Raman Spectra of Molecules and Crystals," Israel Program for Scientific Translations, New York (1972).

6. J. Van Kranendonk, "Solid Hydrogen," Plenum, NY, 1983.

7. W. G. Fateley, F. R. Dollish, N. T. McDevitt, and F. F. Bentley, "Infrared and Raman Selection Rules for Molecular and Lattice Vibrations: The Correlation Method," Wiley, New York (1972).

8. T. A. Scott, "Solid and Liquid Nitrogen," Physics Reports, 27:89 (1976).

9. "International Tables for Crystallography," Vol. A, Second Edition, T. Hahn, ed., Dordrecht, Holland (1987).

10. S. Califano, V. Schettino, and N. Neto, "Lattice Dynamics of Molecular Crystals," Springer-Verlag, Berlin, 1981.

11. For an example of a detailed calculation of factor and site group splittings in benzene, see E. R. Bernstein, S. D. Colson, R. Kopelman, "Electronic and Vibrational Exciton Structure in Crystalline Benzene," J. Chem. Phys. 48:5596 (1968).

12. N. C. Holmes, W. J. Nellis, W. B. Graham, and G. E. Walrafen, "Spontaneous Raman Scattering from Shocked Water," Phys. Rev. Lett. 55:2433 (1985); further references for water under static conditions are given in this paper.

13. D. M. Adams and S. K. Sharma, "Selection of Diamonds for Infrared and Raman Spectroscopy," J. Phys. E 10:680 (1977).

14. R. J. Hemley, P. M. Bell, and H. K. Mao, "Laser Techniques in High Pressure Geophysics," Science 237:605 (1987) and references therein.

15. R. Reichlin, D. Schiferl, S. Martin, C. Vanderborgh, and R. L. Mills, "Optical Studies of Nitrogen to 130 GPa," Phys. Rev. Lett. 55:1464 (1985), and references within.

16. P. M. Bell, H. K. Mao, and R. J. Hemley, "Observations of Solid H_2, D_2, and N_2 at Pressures Around 1.5 MBar at 25° C," Physica 139–140B: 16 (1986), and references within.

17. L. Merrill and W. A. Bassett, "Miniature Diamond Anvil Cell for X-Ray Diffraction Studies," Rev. Sci. Inst. 45:290 (1974).

18. M. Pasternak, J. N. Farrell, and R. D. Taylor, "Metallization and Structural Transformation of Iodine under Pressure: A Microscopic View," Phys. Rev. Lett. 58:575 (1987).

19. A. S. Zinn, D. Schiferl, and M. F. Nicol, "Raman Spectroscopy and Melting of Nitrogen Between 290 and 900 K and 2.3 and 18 GPa," J. Chem. Phys. 87:1267 (1987).

20. A. I. Katz, D. Schiferl, and R. L. Mills, "New Phases and Chemical Reactions in Solid CO Under Pressure," J. Phys. Chem. 88:3176 (1984).

21. D. S. Moore and S. C. Schmidt, "Experimental Molecular Spectroscopy in Shock-Compressed Materials," in: Shock Waves in Condensed Matter, S. C. Schmidt and N. C. Holmes, eds., Elevier Science Publishers, New York (1988).

22. J. W. Nibles and E. V. Knighten, "Coherent Anti-Stokes Raman Spectroscopy" in: "Raman Spectroscopy of Gases and Liquids," A. Weber, ed., Springer-Verlag, Berlin (1979).

23. S. C. Schmidt, D. S. Moore, D. Schiferl, and J. W. Shaner, "Backward Stimulated Raman Scattering in Shock-Compressed Benzene," Phys. Rev. Lett. 50:661 (1983).

24. S. C. Schmidt, D. S. Moore, and M. S. Shaw, "Vibrational Spectroscopy of Fluid N_2 up to 34 GPa and 4400 K," Phys. Rev. B 35:493 (1987).

25. S. C. Schmidt, D. S. Moore, M. S. Shaw, and J. D. Johnson, "Vibrational Spectroscopy of Shock-Compressed Fluid N_2 and O_2," in: Shock Waves in Condensed Matter, S. C. Schmidt and N. C. Holmes, eds., Elevier Science Publishers, New York (1988).

26. Z. H. Yu, D. Strachan, W. B. Daniels, R. Reichlin, S. Martin, and R. L. Mills, private communication.

27. W. M. Tolles, J. W. Nibler, J. R. McDonald, and A. B. Harvey, "A Review of the Theory and Application of Coherent Anti-Stokes Raman Spectroscopy (CARS)," Applied Spectroscopy 31:253 (1977).

28. R. F. Begley, A. B. Harvey, and R. L. Byer, "Coherent Anti-Stokes Raman Spectroscopy," Appl. Phys. Lett. 25:387 (1974).

29. S. C. Schmidt, D. S. Moore, and J. W. Shaner, "Simultaneous Multimode Vibrational Frequency Shift Measurements in Shock-Compressed Organic Liquid Mixtures using Reflected Broad-Band Coherent Anti-Stokes Raman Scattering," Phys. Rev. Lett. 50:1819 (1983).

30. Y.-X. Yan, L.-T. Cheng, and K. A. Nelson, "Impulsive Stimulated Light Scattering," in: Advances in Non-Linear Spectroscopy, R. J. H. Clark and R. E. Hester, eds., John Wiley, New York (1987).

31. M. Baggen, M. van Exter, A. Lagendijk, "Time-Resolved Stimulated Raman Scattering in a Diamond Anvil Cell," J. Chem. Phys. 86:2423 (1987).

32. J. M. Brown, L. J. Slutsky, K. A. Nelson, and L.-T. Cheng, "Velocity of Sound and Equations of State for Methanol and Ethanol to 6.8 GPa in a Diamond-Anvil Cell: An Application of Impulsive Stimulated Scattering," submitted to Science

33. S. F. Agnew, B. I. Swanson, and L. H. Jones, "Extended Interactions in the ε Phase of Oxygen," J. Chem. Phys. 86:5239 (1987) and references therein.

34. D. Schiferl, S. Kinkead, R. C. Hanson, and D. A. Pinnick, "Raman Spectra and Phase Diagram of Fluorine at Pressures up to 6 GPa and Temperatures Between 10 and 320 K," J. Chem. Phys. 87:3016 (1987).

35. P. G. Johansen and W. B. Holzapfel, "Effect of Pressure on Raman Spectra of Chlorine," J. Phys. C. Solid State Phys. 16:L1177 (1983).

36. A. J. Melveger, J. W. Brasch, and E. R. Lippincott, "Laser Raman, Infrared and Visible Spectra of Liquid and Solid Bromine Under High Pressure," Mat. Res. Bull. 4:515 (1969).

37. A. J. Melveger, J. W. Brasch, and E. R. Lippincott, "Laser Raman Spectra of Liquid and Solid Bromine and Carbon Disulfide Under High Pressure," Appl. Optics 9:11 (1970).

38. P. G. Johannsen and W. B. Holzapfel, "Effect of Pressure on Raman Spectra of Solid Bromine," J. Phys. C: Solid State Phys. 16:1961 (1983).

39. O. Shimomura, K. Takemura, and K. Aoki, "Observation of Molecular Dissociation of Iodine at High-Pressure by Raman Scattering Study," in: "Proceedings of the 8th AIRAPT International Conference, Uppsala, Sweden, 1981," C. M. Blackman, T. Johannison, and L. Tegner, eds., Arkitektkopia, Uppsala (1982)

40. R. C. Hanson, "A New High Pressure Phase of Solid CO_2, J. Phys. Chem. 89:1499 (1985), and references within.

41. H. Olijnyk, H. Daufer, H.-J. Jodl, and H. D. Hochheimer, to be published.

42. S. F. Agnew, B. I. Swanson, L. H. Jones, and R. L. Mills, "Disproportionation of Nitric Oxide at High Pressure," J. Phys. Chem. 89:1678 (1985).

43. S. F. Agnew, B. I. Swanson, L. H. Jones, R. L. Mills, and D. Schiferl, "Chemistry of N_2O_4 at High Pressure: Observation of a Reversible Transformation Between Molecular and Ionic Crystalline Forms," J. Phys. Chem. 87:5065 (1983).

...; B. I. Swanson, and D. G. Eckhart, "Spectroscopic Studies of Carbon Disulfide at High Pressure," in: "Shock Waves in Condensed Matter," Y. M. Gupta, ed., Plenum, New York (1986).

45. B. I. Swanson, L. M. Babcock, D. Schiferl, D. C. Moody, R. L. Mills, and R. R. Ryan, "Raman Study of SO_2 at High Pressure: Aggregation, Phase Transformations, and Photochemistry," Chem. Phys. Lett. 91:393 (1982).

46. P. Hebert, A. Polian, P. Loubeyre, and R. LeToullec, "Optical Studies of Methane Under High Pressure," Phys. Rev. B 36:9196 (1987).

47. M. Gauthier, Ph. Pruzan, J. C. Chervin, and J. M. Besson, "Raman Scattering Study of Ammonia up to 75 GPa: Evidence for Bond Symmetrization at 60 GPa," Phys. Rev. B 37:2102 (1988) and references therein.

48. A. Anderson, S. Demoor, and R. C. Hanson, "Raman Study of a New High-Pressure Phase of H_2S," Chem. Phys. Lett. 140:471 (1987).

49. R. C. Hanson and A. Katz, "Solid Hydrogen Chloride at High Pressure," in: "Proceedings of the 9th AIRAPT International Conference, Albany, NY, 1983," C. Homan, R. K. MacCrone, and E. Whalley, eds., North-Holland, NY (1984).

50. A. I. Katz, "High Pressure Studies of the Hydrogen Halides," Thesis, Arizona State University (1987).

51. J. van Straaten and I. F. Silvera, "Vibrational Mode Frequencies, Phase Diagram, and Optical Transmission of Solid HI to 25 GPa," Phys. Rev. B 36:9253 (1987).

52. R. LeSar, S. A. Eckberg, L. H. Jones, R. L. Mills, L. A. Schwalbe, and D. Schiferl, "Raman Spectroscopy of Solid Nitrogen up to 374 kbar," Solid State Comm. 32:131 (1979). For early Raman work on nitrogen at high pressures, see M. M. Thiery, D. Fabre, M. Jean-Louis, and H. Vu, "Raman spectra of solid α-N_2 and γ-N_2 under high pressure at 4.2 K," J. Chem. Phys. 59:4559 (1973) and F. D. Medina and W. B. Daniels, "Raman Spectrum of Solid Nitrogen at High Pressures and Low Temperatures," J. Chem. Phys. 64:150 (1976).

53. D. Schiferl, D. T. Cromer, and R. L. Mills, "Crystal Structure of Nitrogen at 25 kbar and 296 K," High Temp.-High Press. 10:493 (1978).

54. D. T. Cromer, R. L. Mills, D. Schiferl, and L. A. Schwalbe, "The Structure of N_2 at 49 kbar and 298 K," Acta Crystallogr. Sect. B 37:8(1981).

55. D. Schiferl, S. Buchsbaum, and R. L. Mills, "Phase Transitions in Nitrogen Observed by Raman Spectroscopy from 0.4 to 27.4 GPa at 15 K," J. Phys. chem. 89:2324 (1985).

56. S. Nosé and M. L. Klein, "Structural Transformations in Solid Nitrogen at High Pressure," Phys. Rev. Lett. 50:1207 (1983); V. Chandrasekharan, R. D. Etters, and K. Kobashi, "Calculation of High-Pressure Phase Transitions in Solid N_2 and the Pressure Dependence of the Intramolecular Mode Frequencies," Phys. Rev. B 28:1095 (1983); R. LeSar, "Improved Electron-Gas Model Calculations of Solid N_2 to 10 GPa," J. Chem. Phys. 81:5104 (1984);

57. R. L. Mills, B. Olinger, and D. T. Cromer, "Structures and Phase Diagrams of N_2 and CO to 13 GPa by X-ray Diffraction," J. Chem. Phys. 84:2837 (1986).

58. A. K. McMahan and R. LeSar, "Pressure Dissociation of Solid Nitrogen under

1 Mbar," Phys. Rev. Lett. 54:1929 (1985); R. M. Martin and R. J. Needs, "Theoretical Study of the Molecular to Non-Molecular Transformation of Nitrogen at High Pressures," Phys. Rev. B 34:5082 (1986).

59. R. Reichlin, private communication.

60. H. B. Radousky, W. J. Nellis, M. Ross, D. C. Hamilton, and A. C. Mitchell, "Molecular Dissociation and Shock-Induced Cooling in Fluid Nitrogen at High Densities and Temperatures," Phys. Rev. Lett. 57:2419 (1986).

61. R. LeSar, "Vibrational Properties of Dense Molecular Fluids," J. Chem. Phys. 86:4138 (1987); J. Belak, R. D. Etters, and R. LeSar, "Thermodynamic Properties and Equation of State of Dense, Fluid Nitrogen," J. Chem Phys. (in press); R. D. Etters, J. Belak, and R. LeSar, "Thermodynamic Character of the Vibron Frequencies and Equation of State in Dense, High-Temperature N_2," Phys. Rev. B 34:4221 (1986).

62. J. Belak, R. D. Etters, and R. LeSar, unpublished results.

63. R. J. Hemley and R. F. Porter, "Raman Spectroscopy at Ultrahigh Pressures," Scripta Met. 22:139 (1988).

64. H. K. Mao, J. Xu, and P. M. Bell, "Pressure-Induced Infrared Spectra of Hydrogen to 542 kbar," Carnegie Institution Year Book 82:366 (1983).

65. Z. H. Yu, D. Strachan, and W. B. Daniels, private communication.